PHYSICAL REVIEW E **90**, 032901 (2014)

Predictable nonwandering localization of covariant Lyapunov vectors and cluster synchronization in scale-free networks of chaotic maps

Pavel V. Kuptsov[*] and Anna V. Kuptsova

Institute of Electronics and Mechanical Engineering, Yuri Gagarin State Technical University of Saratov, Politekhnicheskaya 77, Saratov 410054, Russia

(Received 20 February 2014; revised manuscript received 22 June 2014; published 2 September 2014)

Covariant Lyapunov vectors for scale-free networks of Hénon maps are highly localized. We revealed two mechanisms of the localization related to full and phase cluster synchronization of network nodes. In both cases the localization nodes remain unaltered in the course of the dynamics, i.e., the localization is nonwandering. Moreover, this is predictable: The localization nodes are found to have specific dynamical and topological properties and they can be found without computing of the covariant vectors. This is an example of explicit relations between the system topology, its phase-space dynamics, and the associated tangent-space dynamics of covariant Lyapunov vectors.

DOI: 10.1103/PhysRevE.90.032901 PACS number(s): 05.45.Jn, 89.75.Hc, 05.45.Ra

I. INTRODUCTION

Localization properties of Lyapunov vectors in spatiotemporal chaotic systems long have attracted interest [1–4]. Recently, this interest has been renewed due to the discovery of algorithms for covariant Lyapunov vectors (CLVs) [5,6]. The evolution of these vectors is governed by linear equations under chaotic forcing, so their localization can be treated as a sort of Anderson localization [2]. The localization sites indicate unstable areas of a system that, in particular, are important for atmosphere dynamics prediction [7]. For homogeneous systems the localization sites of the covariant vectors wander irregularly so their dynamics can be described by the stochastic equation of Kardar-Parisi-Zhang [8,9]. In contrast, the localization positions in inhomogeneous systems are pinned at certain fixed positions [10].

In this paper we analyze properties of CLVs for scale-free networks of chaotic maps. We show that, due to the presence of cluster synchronization, the CLVs are localized. The first mechanism of the localization is related to the full synchronization clusters, and a second one appears due to the existence of large phase-synchronized clusters. Both of the localizations are nonwandering, i.e., nonzero sites of the vectors remain unchanged in the course of the dynamics. Moreover, these nodes have specific topological and dynamical properties so they can be identified without computing the CLVs. This is an example of explicit relations between the system topology, its phase-space dynamics, and the associated tangent-space dynamics of CLVs.

The paper is organized as follows. In Sec. II we introduce the considered network and discuss its dynamics. Section III describes the structure of the tangent space of the network. The mechanism of CLV localization on clusters of full synchronization is described in Sec. IV, and in Sec. V we discuss the localization related to phase clusters. Finally, Sec. VI summarizes the paper results.

[*]Corresponding author: p.kuptsov@rambler.ru

II. MODEL SYSTEM AND CLUSTER SYNCHRONIZATION

A. Dynamical network equations and network structure

We consider a network of Hénon maps build as a generalization of the Hénon chain from Ref. [11] as follows:

$$\begin{aligned} x_n(t+1) &= \alpha - [x_n(t) + \epsilon h_n(t)]^2 + y_n(t), \\ y_n(t+1) &= \beta x_n(t), \end{aligned} \tag{1}$$

$$h_n(t) = \sum_{j=1}^{N} \frac{a_{nj}}{k_n} x_j(t) - x_n(t), \quad k_n = \sum_{j=1}^{N} a_{jn}, \tag{2}$$

where N is the number of network nodes; $t = 0,1,2\dots$ is discrete time; $a_{nj} \in \{0,1\}$, $a_{nn} = 0$ are the elements of the $N \times N$ adjacency matrix $\mathbf{A}$; and k_n is degree of the nth node, i.e., the number of its connections. The parameters controlling local dynamics are $\alpha = 1.4$ and $\beta = 0.3$, and $\epsilon \in [0,1]$ is the coupling strength. The system is time reversible as follows: $x_n(t) = y_n(t+1)/\beta$, $y_n(t) = -\alpha + [y_n(t+1) + \epsilon h'_n(t+1)]^2/\beta^2 + x_n(t+1)$, where $h'_n(t) = \sum_{j=1}^{N} \frac{a_{nj}}{k_n} y_j(t) - y_n(t)$.

We consider random networks with scale-free structure generated via a stochastic process described in Ref. [12]. The process starts from two linked nodes. At each iteration we add one node to the network and one link connecting it with one of the existing nodes. The node to connect is chosen at random with a probability that is proportional to its connectivity degree k_n, i.e, via a so-called preferential attachment mechanism. After $N-1$ steps we obtain a network with N nodes and $N-1$ connections. The node degree distribution for such networks has a power-law shape, $P(k) \sim k^{-3}$. An example of the network is shown in Fig. 5 (this figure is discussed in detail below).

By construction, the networks under consideration do not have loops. It means that starting from any node one cannot return to it without moving back. The networks always have a lot of starlike structures when one hub node is connected with many subordinate ones, like, for example, node 10 in Fig. 5. Moreover, these structures can form a hierarchy; see the hub node 11 that is subordinate with respect to

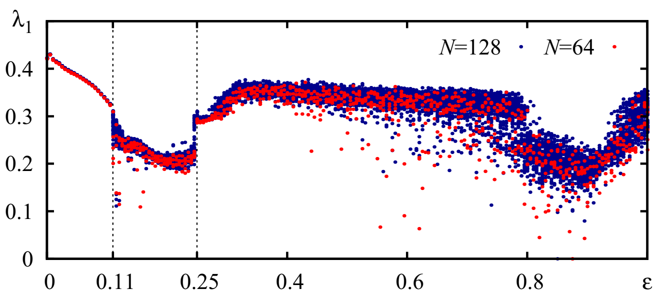

FIG. 1. (Color online) The first Lyapunov exponent vs ϵ for $N = 128$ and 64. Each point is computed independently with a new matrix **A** and initial conditions. At $N = 128$ and 64 there are 50 and 5 points, respectively, for each ϵ. Lines at $\epsilon = 0.11$ and 0.25 delimit the area of interest.

node 10. The structure of considered networks is essentially inhomogeneous. Usually a few nodes are connected with very many others, and many nodes have only one link. All of these properties are found to result in a very long transient time required for the network to arrive at stationary regime. This will be discussed in Sec. II D.

B. The largest Lyapunov exponent

The dynamics of the network (1) is, in general, chaotic. To characterize it we compute Lyapunov exponents using the standard algorithm suggested in Refs. [13,14] (see also Ref. [15] for a review).

Figure 1 shows the largest Lyapunov exponent λ_1 at different coupling strengths. At $\epsilon < 0.11$ the exponent unambiguously depends on ϵ regardless of the network matrix **A**, initial conditions, and the network size. This occurs because the nodes interacts weakly with each others, so the detailed network structure is not very important. The nodes within this area do not demonstrate any concerted oscillations. The area $0.11 < \epsilon < 0.25$ clearly differs from all others. The dependence $\lambda_1(\epsilon)$ is ambiguous here: Every new combination of the network matrix **A** and initial conditions are characterized with their own λ_1. Another feature of this area is lower values of λ_1 with respect to the surrounding areas. This is due to the cluster synchronization emerging here; see the discussion below in Sec. II C. The dependence $\lambda_1(\epsilon)$ remain ambiguous at $\epsilon > 0.25$, although the exponents becomes higher. At $\epsilon > 0.8$ the exponents again become lower so this area is similar to the marked area $0.11 < \epsilon < 0.25$.

In what follows we shall restrict ourselves with the area $0.11 < \epsilon < 0.25$.

C. Full and phase cluster synchronization

Though the synchronization of the whole network is not observed, the nodes can form clusters of synchronized oscillations. Both full and phase synchronization is possible. The former stands for the equivalence of variables at the synchronized nodes, and the latter implies the coincidence of positions of minima and maxima of synchronized time series. The fully synchronized nodes will be referred to as FS clusters, and phase-synchronized nodes will be called Ph clusters.

The phase cluster synchronization of networks nodes is studied in Ref. [16]. According to the approach suggested there, one can detect the Ph clusters computing phase distances. Given a starting time t_0 and a time interval $\mathcal{T}$, count at $t_0 \leqslant t < t_0 + \mathcal{T}$ the numbers ν_m and ν_n of local minima of $x_m(t)$ and $x_n(t)$, respectively, and also find the number ν_{mn} of simultaneous minima of x_m and x_n. Then the phase distance is computed as

$$d_{mn} = 1 - \nu_{mn}/\max(\nu_m,\nu_n). \tag{3}$$

When it vanishes, all the minima of x_m and x_n occur simultaneously and this is the case of phase synchronization of mth and nth nodes over the time interval $\mathcal{T}$. To identify the Ph clusters one can build an auxiliary graph whose nth and mth nodes are linked if $d_{mn} = 0$ and find the clusters as connected components of this graph.

Nonzero d_{mn} is a fraction of time when the nodes m and n are not synchronized. Thus the minimum of d_{mn} over n, i.e.,

$$\tilde{d}_m = \min\{d_{mn} | n = 1 \dots N\}, \tag{4}$$

can be treated as degree of the desynchronization of the mth node with the rest of the network.

The FS clusters can be identified using the matrix of mean absolute differences between dynamical variables over the computation interval $\mathcal{T}$,

$$q_{mn} = \sum_{t=0}^{\mathcal{T}-1} |x_m(t_0 + t) - x_n(t_0 + t)|/\mathcal{T} \tag{5}$$

The FS clusters correspond to connected components of an auxiliary graph whose mth and nth nodes are connected when $q_{mn} = 0$. In actual numerical simulations we considered two nodes as synchronized if $q_{mn} < 10\epsilon_m$, where $\epsilon_m \approx 10^{-16}$ is the machine epsilon for double precision variables that was employed.

The length of the interval $\mathcal{T}$ for which the cluster detection is performed can influence the resulting picture. As we discuss in this section below and in Sec. II D, there exist so-called floating nodes that intermittently can either belong to one of the Ph clusters or oscillate separately. With a large $\mathcal{T}$ we consider clusters including only permanent nodes, while performing a serial cluster detections with a small $\mathcal{T}$ we can take into account fluctuations arising due to the floating nodes.

Figure 2 illustrates the cluster synchronization of networks with $N = 64$, 128, and 256 nodes that is observed at different ϵ. Figures 2(a) and 2(b) show rescaled sizes

$$S_p^* = S_p/N, \quad S_f^* = S_f/\sqrt{N} \tag{6}$$

of three largest Phand FS clusters, respectively. Figures 2(c) and 2(d) represent rescaled numbers,

$$M_p^* = M_p/N, \quad M_f^* = M_f/N, \tag{7}$$

of nodes attached to all Phand FS clusters, respectively. Figures 2(e) and 2(f) show rescaled numbers,

$$N_p^* = N_p/N, \quad N_f^* = N_f/N, \tag{8}$$

of Ph and FS clusters, respectively. The clusters appears at $\epsilon = 0.11$. As one can see in Fig. 2(a) in the area $0.11 < \epsilon < 0.25$ there are two large Ph clusters whose relative sizes are $S_p^* \approx 0.4{-}0.5$. The rescaled curves in Fig. 2(e) plotted for

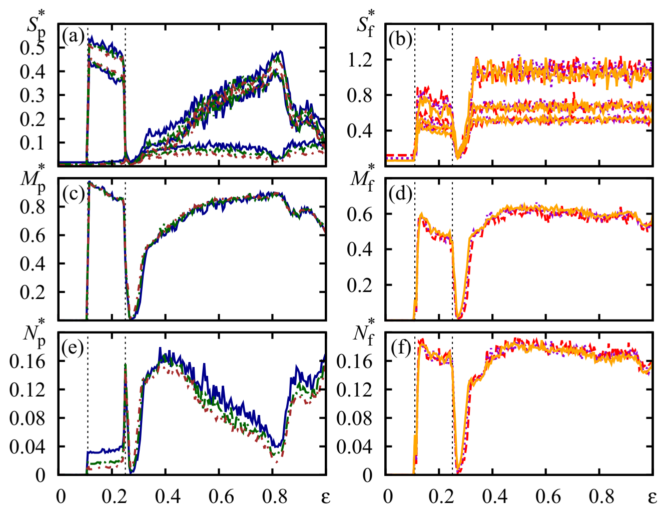

FIG. 2. (Color online) [(a) and (b)] Rescaled sizes of three largest Ph and FS clusters, see Eq. (6). [(c) and (d)] Rescaled numbers of nodes attached to all Ph and FS clusters, see Eq. (7). [(e) and (f)] Rescaled numbers of Ph and FS clusters, see Eq. (8). All values are averaged over 25 computations with different matrices **A** and initial conditions at each ϵ. $\mathcal{T} = 10\,000$. Different curves in each panel correspond to $N = 62$, 128, and 256. Vertical dotted lines are plotted at $\epsilon = 0.11$ and 0.25 to delimit the area of interest.

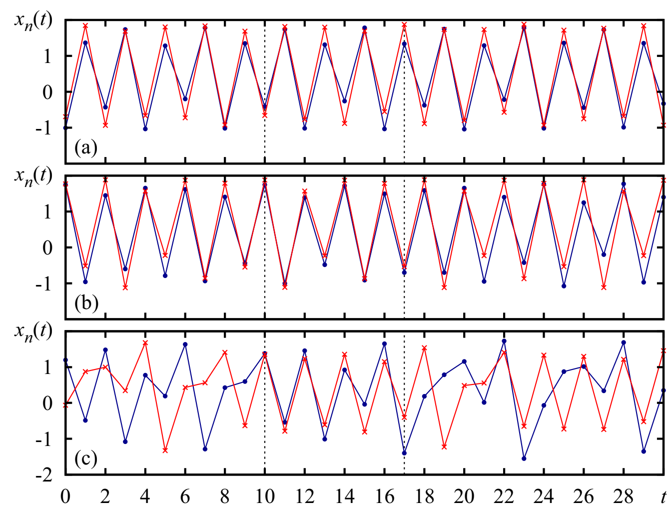

FIG. 3. (Color online) [(a) and (b)] Oscillations at nodes belonging to two large Ph clusters. (c) Separated nodes not synchronized with others. Vertical dotted lines delimit the interval when both separated nodes in panel (c) are attached to the cluster represented in panel (b). $N = 128$, $\epsilon = 0.17$.

different N do not coincide, but pure curves plotted without the rescaling are found to be the same (not shown), i.e., the number of Ph clusters does not depend on N. Since $S_p \sim N$, see Eq. (6), regardless of N, these clusters includes the bulk of nodes. However, as follows from Fig. 2(c) and Eq. (7), the Ph clusters include at any N approximately 85% of the nodes, so there are always nodes that are not synchronized with Ph clusters.

Despite the Ph clusters, the number of FS clusters scales as $N_f \sim N$ and the total number of nodes attached to all FS clusters grows as $M_f \sim N$. It presumes that the mean size of FS nodes is constant. However, the size of the largest cluster grows: At $N = 64$, 128, and 256 the sizes are $S_f \approx 6$, 9, and 13, respectively. According to Eq. (6), the sizes of the largest FS clusters scales with N as $S_f \sim \sqrt{N}$.

At the right boundary of the discussed area at $\epsilon = 0.25$ the large Ph clusters disintegrate into many small ones; see the spike of N_p^* in Fig. 2(e). Moreover, in this area N_p starts to scale as $N_p \sim N$. As ϵ further grows all clusters disappears but then their number again increases. Notice the identical behavior of curves in Figs. 2(c) and 2(e) and Figs. 2(d) and 2(f), respectively, around $\epsilon \approx 0.3$. It indicates the presence here of FS clusters only. Subsequent growth of ϵ results in the reappearance of the Ph clusters, but their number is still high. At $\epsilon \approx 0.4$ the number of Ph clusters starts to decay, Fig. 2(e), and the number of the attached nodes increases, Fig. 2(c). Also observe the growth of the first two largest clusters, Fig. 2(a). As for the FS clusters, their sizes, Fig. 2(b), the number of attached nodes, Fig. 2(d), and their total number, Fig. 2(f), remains approximately unchanged. At $\epsilon \approx 0.8$ one again observes the situation when there are two large Ph clusters and many small FS clusters. But, contrary to the area $0.11 < \epsilon < 0.25$, this area is much narrower and when ϵ gets larger the disintegration of Ph clusters occurs within the wider range of ϵ. As already mentioned above, we shall consider the dynamics of the network within the area at $0.11 < \epsilon < 0.25$.

Figure 3 illustrates behavior of synchronized and separated nodes, Figs. 3(a), 3(b), and 3(c), respectively, within the area of interest, when almost all nodes belong to two large Ph clusters. Observe in Figs. 3(a) and 3(b) strict alternations of maxima and minima of variables attached to Ph clusters and irregular variations of their amplitudes. Also compare Figs. 3(a) and 3(b): The oscillations of Ph clusters have opposite phases. The separated nodes, Fig. 3(c), oscillate irregularly; however, for some time they can be attached to one of the clusters, see area $25 < t < 30$ in Fig. 3(c).

If a node spends an essential part of the time being synchronized with others but loses the synchronization intermittently, it will be called "floating," according to the notation suggested in Ref. [16].

D. Convergence of the cluster structure

The network (1) converges very slowly to its stationary regime. As one can see in Fig. 4, the relative numbers M_p^* and M_f^* of nodes attached to Ph and FS clusters, respectively, can change even after a very long evolution time. Since in this figure the clusters are identified over the intervals $\mathcal{T} = 100$, the total evolution time of the system is $t = 10^6$. The represented examples are not very typical in a sense that we tried approximately 10 different matrices **A** and initial conditions for each ϵ to show the cases with the worst convergence. However, the convergence in other cases is not much faster. Nevertheless, in Fig. 4 and in all other cases that we tried the curves always behaved as if they approached limiting values. Thus we can conjecture that the stationary regime exists and it takes a long transient time to approach it, $t_{\text{trans}} = 5 \times 10^5 N/64$.

Observe frequent peaks and dips on the curves for M_p^*, see Fig. 4(a). They appear due to the floating nodes that

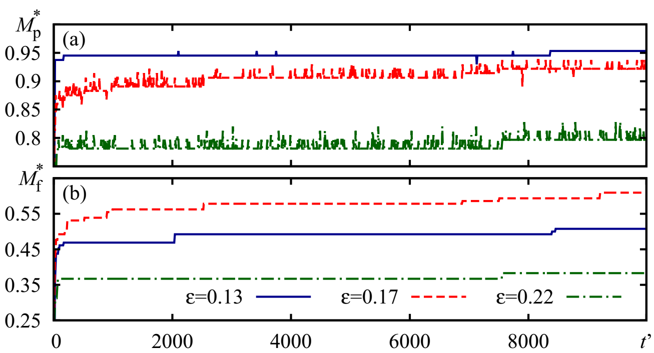

FIG. 4. (Color online) Convergence of the (a) Ph and (b) FS clusters. t' enumerates the cluster detection procedures performed over the intervals $\mathcal{T} = 100$ in the course of the evolution of the system. $N = 128$, $\epsilon = 0.13, 0.17$, and 0.22.

intermittently attach and detach the Ph clusters. The floating nodes exist only with respect to Ph clusters; if a node gets attached to a FS cluster it stays synchronized permanently, see Fig. 4(b).

Curves in Fig. 4(a) can be treated as a highly fluctuating signal. However, the observed fluctuations appear due to the serial cluster detection with sufficiently short $\mathcal{T}$. One can change the definition of observable variables and perform the clusters detected just once over the whole computation time. The clusters defined in this way are stationary, but also there are noncluster nodes oscillating chaotically. Below we shall employ both approaches.

E. An example of the network

It is useful to enumerate the network nodes according to the cluster structure. First, we find Ph and FS clusters and enumerate them with indexes $i \in [0 \dots N_p]$ and $j \in [0 \dots N_f]$, respectively, in ascending order of their sizes, where N_p and N_f are the numbers of corresponding clusters. The index 0 indicates trivial clusters including a single node only. Then the nodes are assigned the indexes i_m and j_m in accordance to their membership in clusters, and the desynchronization degree $\tilde{d}_m$ is computed for them, see Eq. (4). Now the real-valued clustering index is defined as

$$\eta_m = \begin{cases} -\tilde{d}_m & \text{if} \quad \tilde{d}_m > 0, \\ i_m + j_m/(N_f+1) & \text{if} \quad \tilde{d}_m = 0. \end{cases} \tag{9}$$

Finally, the nodes are enumerated in the ascending order of η_m. The negative η_m indicates that the corresponding node is not synchronized with others, and if, in addition, η_m is very close to zero the corresponding node is the floating one. The integer part of positive η_m is the index of the Ph cluster to which the node belongs and the fractional part encodes the FS cluster index.

Figure 5 shows an example of the network structure as well as its Ph and FS clusters that have emerged in the course of the evolution. The nodes are enumerated according to the ascending order of η_m that is plotted in Fig. 9(a). The cluster detection is performed over the whole computation interval 10^5.

For this particular case there are five nodes that are not synchronized with others, i.e., have $\eta_m < 0$. The first two of them are essentially separated, $\eta_{1,2} \approx -0.16$, and the nodes 3, 4, and 5 are the floating ones with very small $|\eta_m|$: $\eta_3 = -0.00054$, $\eta_4 = -0.00028$, $\eta_5 = -2 \times 10^{-5}$.

The bulk of nodes form two large Ph clusters. In our case, for these clusters $3 \leqslant \eta_m < 4$ and $4 \leqslant \eta_m < 5$, see Fig. 9(a). As one can see in Fig. 5, there is no visible relation between the connectivity structure of the network and the locations of

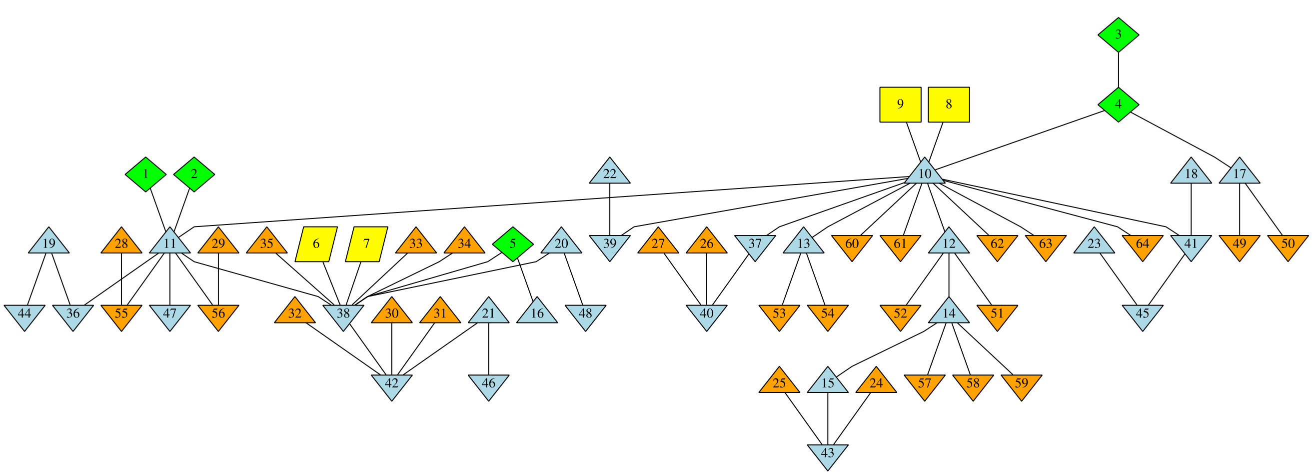

Separated nodes / floating	1, 2, 3, 4, 5 / 3, 4, 5	green diamonds
Separated FS-clusters	{6,7}, {8,9}	yellow filling
Large Ph-clusters	{10–35}, {36–64}	upturned and downturned triangles
FS-clusters embedded into large Ph-clusters	{24,25}, {26,27}, {28,29}, {30,31,32}, {33,34,35}, {49,50}, {51,52}, {53,54}, {55,56}, {57,58,59}, {60,61,62,63,64}	orange filling

FIG. 5. (Color online) An illustration of the clustering of network (1) with $N = 64$ and $\epsilon = 0.17$. The nodes and edges represent the connectivity structure and the shapes and colors of nodes indicate the states arrived in course of the evolution, see the table below the graph. To plot this figure we collected data for the cluster identification over $\mathcal{T} = 10^5$ steps.

these clusters. The cluster nodes are mixed so many nodes of the first cluster are connected with others only through elements of the second one and vice versa. As we mentioned above, see Figs. 3(a) and 3(b), the oscillations within these clusters have opposite phases. Thus, in a wider sense, one can say that all nodes of these two clusters are phase synchronized but some with a phase shift.

Some of nodes of the Ph clusters are synchronized stronger so they form FS clusters embedded into Ph clusters. For these clusters η_m is fractional and $\eta_m > 3$. Observe that all of these clusters are formed by elements of starlike structures and all interactions inside FS clusters pass through hub nodes. The hub nodes in turn are never synchronized with their subordinate nodes; see, for example, the cluster {24,25} connected through a hub 43. Moreover, the hub always belongs to the opposite Ph cluster: observe different orientations of the triangles representing the cluster nodes and the corresponding hubs. This type of synchronization was first reported in Ref. [16] for clusters of phase synchronization. The authors called it driven synchronization. Later this mechanism was independently described in Refs. [17,18] and referred to as "remote synchronization."

The structures mentioned so far are typical and always exist for any **A** and initial conditions. In some cases, however, like, for example, the one shown in Fig. 5, several more small FS clusters appear that are separated from two large Ph clusters: the nodes 6 and 7 are fully synchronized with each other but are not embedded into Ph clusters. The same is the case for the nodes 8 and 9.

Finally, notice that remote synchronization can also occur when "beams" of a starlike structure include two edges. The nodes 28 and 29 form a FS cluster, but they can interact only through the nodes 55 and 56. The latter ones are also synchronized. The opposite orientation of the corresponding triangles indicates that these clusters are embedded into different Ph clusters. This situation can be treated as remote synchronization of the second order.

III. STRUCTURE OF THE TANGENT SPACE

A. The Jacobian matrix

The Jacobian matrix of the network (1) has a block form being composed of $N \times N$ matrices,

$$\mathbf{J}(t) = \begin{pmatrix} \mathbf{F}(t) & \mathbf{I} \\ \beta \mathbf{I} & 0 \end{pmatrix}, \tag{10}$$

where

$$\mathbf{F}(t) = -2\mathbf{G}(t)\,[(1-\epsilon)\mathbf{I} + \epsilon \mathbf{K}^{-1}\mathbf{A}],$$
$$\mathbf{G}(t) = \mathrm{diag}\{x_n + \epsilon h_n\}, \quad \mathbf{K} = \mathrm{diag}\{k_n\}, \tag{11}$$

and **I** is the identity matrix. $\mathbf{J}(t)$ has a generic symplectic structure, i.e., at any t there exists a skew-symmetric matrix $\mathbf{W}(t)$ such that $\mathbf{J}(t)\,\mathbf{W}(t)\,\mathbf{J}(t)^T = -\beta\mathbf{W}(t)$. Systems of this type were first introduced in Ref. [19]; however, unlike the referenced paper in our case, $\mathbf{W}(t)$ is a generic skew-symmetric matrix depending on t,

$$\mathbf{W}(t) = \begin{bmatrix} 0 & -\mathbf{Q}(t) \\ \mathbf{Q}(t) & 0 \end{bmatrix}, \tag{12}$$

where $\mathbf{Q}(t)$ is a symmetric matrix such that the product $\mathbf{F}(t)\mathbf{Q}(t) = \mathbf{M}(t)$ is also symmetric. $\mathbf{Q}(t)$ can always be found since any matrix $\mathbf{F}(t)$ can always be represented as the product of two symmetric matrices, $\mathbf{F}(t) = \mathbf{M}(t)\mathbf{Q}(t)^{-1}$ [20]. Due to the this property the Lyapunov spectrum is symmetric [19]:

$$\lambda_n + \lambda_{N+1-n} = \log\beta. \tag{13}$$

The Lyapunov spectra for our system are shown in Fig. 7 and discussed below.

B. Pairwise orthogonal eigensubspaces of the tangent space

In the presence of FS clusters the tangent space of the network (1) is split into $N_f + 1$ time-invariant subspaces that are pairwise orthogonal, where N_f is the number of FS clusters. There are N_f subspaces representing perturbations transverse to manifolds where the FS clusters belong, and the one that includes perturbations longitudinal to all of these manifolds.

Consider a toy network, see Fig. 6. Its first and second nodes are linked with the third one to form a starlike structure and the first FS cluster. The fifth, sixth, and seventh nodes form the second FS cluster. The top left block of the corresponding Jacobian matrix has the following form, see Eq. (10):

$$\mathbf{F} = \begin{pmatrix} G_1\epsilon' & 0 & G_1\epsilon & 0 & 0 & 0 & 0 \\ 0 & G_1\epsilon' & G_1\epsilon & 0 & 0 & 0 & 0 \\ \frac{1}{3}g_3\epsilon & \frac{1}{3}g_3\epsilon & g_3\epsilon' & \frac{1}{3}g_3\epsilon & 0 & 0 & 0 \\ 0 & 0 & \frac{1}{4}g_4\epsilon & g_4\epsilon' & \frac{1}{4}g_4\epsilon & \frac{1}{4}g_4\epsilon & \frac{1}{4}g_4\epsilon \\ 0 & 0 & 0 & G_2\epsilon & G_2\epsilon' & 0 & 0 \\ 0 & 0 & 0 & G_2\epsilon & 0 & G_2\epsilon' & 0 \\ 0 & 0 & 0 & G_2\epsilon & 0 & 0 & G_2\epsilon' \end{pmatrix}, \tag{14}$$

where $\epsilon' = 1 - \epsilon$, g_i are elements of the matrix $(-2\mathbf{G})$, see Eq. (11), and $g_1 = g_2 = G_1$, $g_5 = g_6 = g_7 = G_2$ correspond to FS clusters.

Due to the special form of **F** there exist vectors of three types, whose structure is preserved under the mapping with **F**

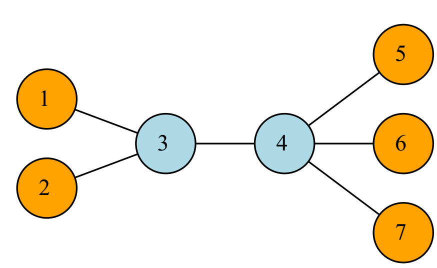

FIG. 6. (Color online) A toy network with two starlike structures. The orange color marks the nodes subjected to the remote synchronization.

as follows:

$$\vec{v}^{\,(0)} = \left(v_1^{(0)}, v_2^{(0)}, v_3^{(0)}, v_4^{(0)}, v_5^{(0)}, v_6^{(0)}, v_7^{(0)}\right)^T, \quad v_1^{(0)} = v_2^{(0)}, \quad v_5^{(0)} = v_6^{(0)} = v_7^{(0)}, \tag{15}$$

$$\vec{v}^{\,(1)} = \left(v_1^{(1)}, v_2^{(1)}, 0,0,0,0,0\right)^T, \quad v_2^{(1)} + v_1^{(1)} = 1, \tag{16}$$

$$\vec{v}^{\,(2)} = \left(0,0,0,0, v_5^{(2)}, v_6^{(2)}, v_7^{(2)}\right)^T, \quad v_5^{(2)} + v_6^{(2)} + v_7^{(2)} = 0. \tag{17}$$

The subspaces spanned by these vectors, $\mathbb{F}_j = \mathrm{span}\{\vec{v}^{\,(j)}\}$, where $j = 0,1,2$, are invariant with respect to $\mathbf{F}$ and thus form the eigensubspaces of $\mathbf{F}$. Moreover, any vector of the form $\vec{v}^{\,(1)}$ and $\vec{v}^{\,(2)}$ is the eigenvector of $\mathbf{F}$ with the eigenvalues $G_{1,2}(1-\epsilon)$. Notice that all these three subspaces are pairwise orthogonal, i.e., the orthogonal are any two vectors from these subspaces.

The full Jacobian matrix $\mathbf{J}$, see Eq. (10), also has three eigensubspaces $\mathbb{J}_j = \mathrm{span}\,\{\vec{w}^{\,(j)}\}$ spanned by the following block vectors:

$$\vec{w}^{\,(j)} = \begin{pmatrix} \vec{v}_x^{\,(j)} \\ \vec{v}_y^{\,(j)} \end{pmatrix}, \tag{18}$$

$j = 0,1,2$. Here $\vec{v}_x^{\,(j)}$ and $\vec{v}_y^{\,(j)}$ are the vectors with the structures (15)–(17), related to perturbations to x and y components of the system. The dimensions of these subspaces are twice the dimensions of the eigensubspaces of $\mathbf{F}$. One can find explicitly a couple of corresponding eigenvectors for subspaces $\mathbb{J}_1$ and $\mathbb{J}_2$,

$$\vec{w}_\pm^{\,(j)} = \vec{v}^{\,(j)} \begin{pmatrix} 1 \\ \beta/\mu_\pm^{(j)} \end{pmatrix}, \tag{19}$$

where $\vec{v}^{\,(j)}$, $j = 1,2$, are arbitrary vectors with the structure (16) and (17), respectively, and $\mu_\pm^{(j)}$ are the corresponding eigenvalues,

$$\mu_\pm^{(j)} = \left(G_j(1-\epsilon) \pm \sqrt{G_j^2(1-\epsilon)^2 + 4\beta}\right)/2. \tag{20}$$

For the considered toy network the eigenvalues $\mu_+^{(1)}$ and $\mu_-^{(1)}$ both have the multiplicity 1, and the multiplicity of $\mu_+^{(2)}$ and $\mu_-^{(2)}$ is 2.

The subspaces $\mathbb{J}_1$ and $\mathbb{J}_2$ include perturbations transverse to invariant manifolds of FS clusters. The dimensions of these subspaces are 2 and 4, respectively. All vectors from $\mathbb{J}_0$ contain identical values at sites corresponding to the same FS cluster, see Eq. (15). It means that these vectors describe perturbations longitudinal to FS-cluster manifolds also affecting noncluster nodes. The dimension of $\mathbb{J}_0$ is 8. All three subspaces are orthogonal to each other.

In the general case the tangent space of the dynamical network under consideration is split into a set of eigensubspaces $\mathbb{J}_j$ of $\mathbf{J}$, where $0 \leqslant j \leqslant N_f$, and N_f is the number of FS clusters. These subspaces are time invariant and pairwise orthogonal. The subspace $\mathbb{J}_j$, where $j \geqslant 1$, represents perturbations transverse to the jth cluster. It is spanned by vectors having only $2S_j$ nonzero sites corresponding to x and y variables at cluster nodes, where S_j is the size of the cluster. Since the sums along x and along y sites have to be zero, the dimension of this subspace, i.e., the number of independent vectors, is $2(S_j - 1)$. The subspace $\mathbb{J}_0$ is spanned by vectors of longitudinal perturbations to FS clusters. These vectors have identical values at sites corresponding to each node and independent values at other sites. The dimension of this subspace is $2(N - M_f + N_f)$, where M_f is the total number of nodes belonging to all FS clusters.

IV. NONWANDERING LOCALIZATION OF CLVs ON FS CLUSTERS

A. The mechanism of localization

Let $\boldsymbol{\Gamma}(t)$ be a $2N \times 2N$ matrix whose columns are CLVs at time t. By the definition, this is a unique set of vectors such that for any t the Jacobian matrix $\mathbf{J}(t)$ maps $\boldsymbol{\Gamma}(t)$ to $[\mathbf{C}(t+1)\,\Gamma(t+1)]$, where $\mathbf{C}(t)$ is a diagonal matrix logarithms of whose elements are finite time Lyapunov exponents [15]. In other words, the tangent-space operator, which is $\mathbf{J}$ for discrete time systems, maps each CLV at t to the stretched or contracted CLV at $t+1$.

The direct sum of the subspaces $\mathbb{J}_j, 0 \leqslant j \leqslant N_f$, is equal to the whole tangent space, and the subspaces are time invariant and, moreover, pairwise orthogonal. Thus each of them holds a set of CLVs related to perturbations to individual clusters or to noncluster nodes. The number of these vectors is equal to the dimension of the corresponding subspace $\mathbb{J}_j$. These CLVs can freely evolve only within their subspaces and never leave them. Let us assume that this is not the case and there exists a probe CLV not fully belonging to one of the subspaces $\mathbb{J}_j$. This vector can always be decomposed into a linear combination of vectors from $\mathbb{J}_j$. In the course of the evolution the vectors of this decomposition grow or decay exponentially, on average, but always stay within their subspaces. The rates of this growth or decay are the Lyapunov exponents. One of the vectors with the largest Lyapunov exponent will always dominate all others so our probe CLV will fall into the corresponding subspace. Thus each CLV indeed belongs to one of $\mathbb{J}_j$. In principle, however, the Lyapunov exponents from different subspaces can coincide. In this case the corresponding CLVs will be linear combinations of vectors from these subspaces.

The CLVs related to transverse perturbations of FS clusters have nonzero elements only at sites corresponding to the cluster nodes. Since the considered FS clusters are small, the corresponding CLVs are highly localized. Moreover, this localization is nonwandering, i.e., the nonzero vector elements always have a fixed location.

Localization of CLVs is a well-known phenomenon. However for chainlike systems whose nodes have identical patterns of connections the localization sites wander around irregularly from node to node [8,9]. The nonwandering localization of CLVs is known to occur due to the inhomogeneous structure of a system. It was already reported for a disordered medium in Ref. [10]. From a general point of view the nonwandering localization of CLVs in our system also occurs because the system is highly inhomogeneous, namely due to the starlike structures when there are highly connected hubs and low connected subordinate nodes.

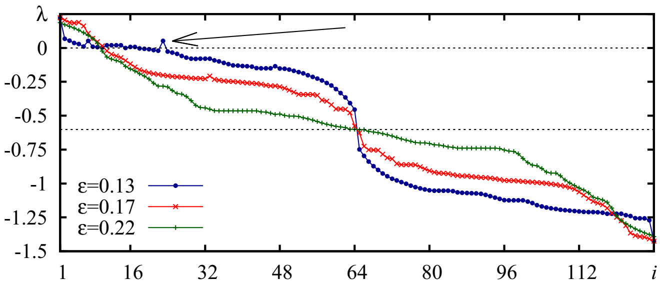

FIG. 7. (Color online) Lyapunov spectra of the network (1) with various coupling strengths, $\epsilon = 0.13, 0.17,$ and 0.22. The upper dotted line marks zero, while the lower one is the symmetry axis at $(\log\beta)/2$. The arrow points an example of anomalous behavior. $N = 64$.

B. Defects of Lyapunov spectra

Let us consider the Lyapunov spectra of the network (1), see Fig. 7. Observe the symmetry of the curves, emerging due to the generic symplectic structure of the Jacobian matrix, see Eq. (13). The theory behind the algorithm for Lyapunov exponents [13,14] is based on the hierarchy of domination of tangent vectors obeyed by different Lyapunov exponents. During the computation we evolve a set of tangent vectors mapping them with the Jacobian matrix and thus allowing alignment along the most expanding available directions. To exclude the alignment of all the vectors along the same directions, we periodically orthogonalize them. So the first one points to the most expanding direction, and the second one, as well as all others, are orthogonal to it and can only align along the second expanding direction, and so on. The average exponential growth rates of these vectors are the Lyapunov exponents. Obviously they have to appear in a nonascending order.

However, in our case the nonascending order can be broken; see the arrow in Fig. 7. Notice the absence of the symmetrical defect on the second part of the spectrum. This abnormal behavior is related to the splitting of the tangent space into the orthogonal subspaces $\mathbb{J}_j$. Right after the start of the iterations, the tangent vectors have random directions. If the local expansion rates for some of the subspaces $\mathbb{J}_j$ highly deviate from the corresponding Lyapunov exponents, this subspace can attract wrong vectors. In the "normal" situation the wrong orientation of vectors is fixed after a transient time when the influence of local rates decays. But in our case, since the subspaces $\mathbb{J}_j$ are time invariant, the vectors can be trapped within inappropriate subspaces. As a result, we observe the broken order of Lyapunov exponents as shown by the arrow in Fig. 7.

One can try to avoid this trapping by adding a small noise to tangent vectors after each iteration. The noise is expected to push out the vectors from their traps, giving them a chance to arrive at the appropriate subspace. Our tests showed that even very small noise of the order 10^{-10} can smoothen the defects of Lyapunov spectra. However, instead of the pushing out of the trapped vectors, the noise destroys the splitting of the tangent space at all. The vectors no longer gain the structures described by Eqs. (15)–(17). Thus this is an inappropriate approach since the existence of the tangent subspaces $\mathbb{J}_j$ is one of the essential features of our system.

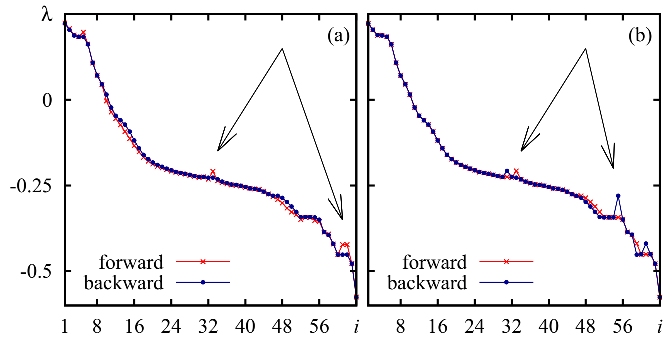

FIG. 8. (Color online) Lyapunov spectra computed in parallel with computation of CLVs via the (a) IR and (b) LU methods. Two curves in the panels correspond to the exponents computed in course of forward- and backward-time stages. The arrows show the essential deviations of the curves from each other.

C. Structure of CLVs

Now we turn to the CLVs. There are two numerical methods for computing CLVs that have been published simultaneously. The method reported in Ref. [5] shall be referred to as the IR method (the abbreviation stands for "Iterations with R matrices"). It computes CLVs in the course of iterations backward in time with inverted upper triangle matrices **R** previously obtained on the forward-time stage as a result of so-called QR matrix decompositions. The other method first reported in Ref. [6] was later improved in Ref. [9] and then it was reformulated in a more efficient form in Ref. [15]. This method shall be referred to as the LU method since it computes CLVs as a result of LU decomposition of matrices of scalar products of orthogonal Lyapunov vectors computed in the course of forward- and backward-time procedures.

Both of the methods for CLVs include the iterations with tangent vectors forward and backward in time. To compute CLVs correctly, these iterations have to provide the identical orderings of tangent vectors, even if this does not correspond to the nonascending order of the Lyapunov exponents. Unfortunately the trapping of vectors within inappropriate subspaces $\mathbb{J}_j$ can occur independently and thus differently on forward and backward stages. These situations can be identified by comparing Lyapunov exponents computed in parallel with forward and backward stages; see Fig. 8. One can see that, besides natural small and smooth deviations, related to an unavoidable numerical noise, there are points marked by arrows where the orders of the exponents do not coincide. It indicates that the forward- and backward-time data do not exactly match so the corresponding CLVs are not quite correct. These abnormal deviations of the curves are found to be is less pronounced for the IR method, and below we shall use it for computing CLVs.

Figure 9(b) shows CLVs averaged in time. Since two variables are associated with each node, we consider the node-related CLVs $p_{ni} = \gamma_{2n-1,i}^2 + \gamma_{2n,i}^2$, where γ_{ji} is the jth element of the ith CLV, $i,j = 1,\ldots,2N$, $n = 1,\ldots,N$. Because each CLV has a unit length, $\sum_{n=1}^{N} p_{ni} = 1$ for any i. Figure 9 corresponds to the network shown in Fig. 5. The nodes of the network are enumerated according to the ascending

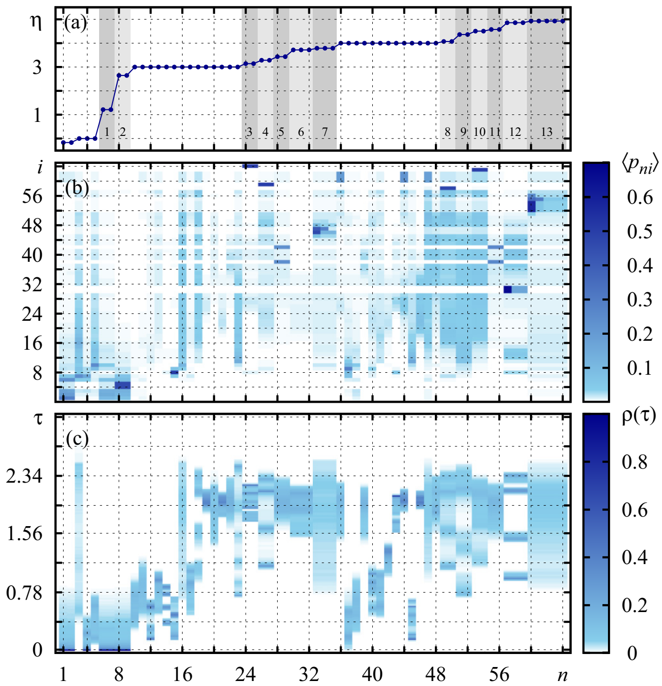

FIG. 9. (Color online) (a) Clustering index η_n, see Eq. (9). The nodes are enumerated according to the ascending order of η_n. Gray labeled stripes indicate FS clusters. (b) Average node-related CLVs. (c) Distributions of τ_n, see Eq. (23). For all panels n is the node number and i is the vector number. $N = 64$, $\epsilon = 0.17$. The matrix **A** and initial conditions are the same as in Fig. 5.

order of η_n, see Eq. (9). The curve η_n is shown in Fig. 9(a). Gray stripes in this panel mark FS clusters.

According the discussion above, there are CLVs localized in FS clusters. The most clear examples correspond to the clusters 3, 4, 7, 8, 10, 12, and 13. The number of vectors has to be 1 less then the number of nodes in the cluster (notice that only the first part of the symmetric spectrum is shown, and one more set of vectors also exist in the second part). Thus each of the two-node clusters 3, 4, 8, and 10 produces a single localized CLV. The three-node clusters 7 and 12 generate pairs of CLVs. Finally, the five-node cluster 13 is characterized by four CLVs.

The two-node clusters 5 and 11 generate two CLVs, localized simultaneously on both of these clusters. These clusters includes the nodes {28, 29} and {55,56}, respectively. As we already discussed above, they demonstrate remote synchronization of the second order, since the nodes 28 and 29 are synchronized through the nodes 55 and 56, see Fig. 5. Due to this reason the exponential growth rates in the subspaces corresponding to these two clusters are always identical and no one of them dominates. The resulting CLVs are linear combinations of vectors localized on these clusters.

The clusters 1, 2, 6, and 9 are problematic. The two-node cluster 2 has two localized CLVs instead of the expected one, and the clusters 1, 6, and 9 do not have any clearly localized CLVs. We addressed the issues regarding the failure of the numerical methods due to the trapping of tangent vectors within inappropriate subspaces $\mathbb{J}_j$ above.

All CLVs not localized on FS clusters belong to $\mathbb{J}_0$, representing longitudinal perturbations to these clusters. It means that they have to have identical values at sites corresponding to FS clusters. One can see that this requirement is fulfilled well even for problematic clusters.

V. NONWANDERING LOCALIZATION OF CLVs ON NODES SEPARATED FROM Ph CLUSTERS

A. Properties of localized vectors

Besides the localization on FS clusters one can also observe in Fig. 9(b) that the first six vectors are localized on nodes 1, 2, and 6–9. The common property of these nodes is that they do not belong to Ph clusters, see Fig. 5.

To clarify it, we shall detect the clusters at $\mathcal{T} = 20$. Since the oscillations of phase-synchronized nodes are very close to periodic with the period 2, see Fig. 3, this short $\mathcal{T}$ is the smallest reasonable value required to identify intermittent attachments and detachments of nodes to Ph clusters. Running over the computation interval and performing serial detections of Ph clusters we assign to each node at each time step a flag signalling whether this node belongs to a Ph cluster or not. Also we compute CLVs and for each vector at each time step using the flags we find a sum,

$$p_s(t) = \sum_{n=1}^{M_s(t)} p_{ni}(t), \tag{21}$$

where $M_s(t)$ is the number of nodes separated from the Ph clusters. The nodes in this equations are assumed to be enumerate in a such a way that the separated nodes go first. Since $\sum_{n=1}^{N} p_{ni} = 1$, p_s indicates what a fraction of nonzero CLV elements belongs to the separated nodes. The upper limit $p_s = 1$ tells that all nonzero CLV elements are localized on separated nodes, while $p_s = 0$ shows that all nonzero CLV elements are localized on Ph clusters.

The distributions of p_s are found to have two maxima, one at $p_s = 0$ and the other at $p_s = 1$, and they decay fast towards to the middle area. Figure 10 plotted for the network in Figs. 5 and 9 shows that the decays near both edges are obeyed to power laws. Notice that the orders of the curves representing different vectors differ at the left and right edges. For the vector $i = 1$ $\rho(0) < \rho(1)$. It means that this vector is

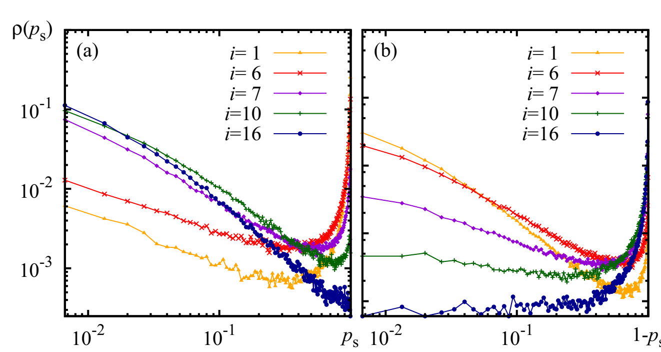

FIG. 10. (Color online) Power-law decays of $\rho(p_s)$ (a) near $p_s = 0$ and (b) near $p_s = 1$. Double logarithmic scales are used for both axes. The vector numbers are shown in the legends. The matrix **A** and initial conditions are the same as in Figs. 5 and 9.

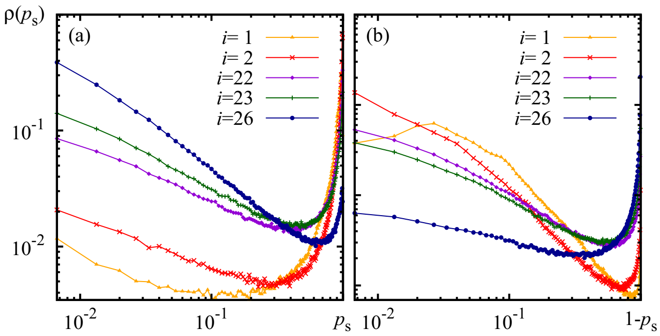

FIG. 11. (Color online) Distributions $\rho(p_s)$ at $N = 128$, $\epsilon = 0.22$.

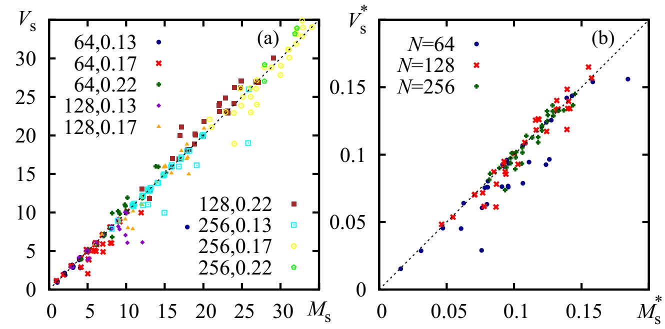

FIG. 12. (Color online) (a) The number of nodes nonsynchronized with the Ph clusters M_s vs the number of CLVs V_s localized on them. The legend shows the values of $N = 64$, 128, and 256 and $\epsilon = 0.13$, 0.13, and 0.22. (b) Rescaled values M_s^* vs V_s^*, see Eq. (22) for $N = 64$, 128, and 256 at $\epsilon = 0.17$.

preferably localized on nodes not attached to the Ph clusters. This is also the case for all vectors up to the sixth one, while for the seventh vector we observe $\rho(0) > \rho(1)$. Starting from this vector, all other CLVs are preferably localized on the nodes attached to the Ph clusters.

Figure 11 shows the distributions $\rho(p_s)$ at $N = 128$ and $\epsilon = 0.22$. One again observes the power laws near the edges and preferable localization of the vectors $1 \leqslant i \leqslant 22$ on the nodes not attached to the Ph clusters, since for these vectors $\rho(0) < \rho(1)$. Also notice the essential deviation from the power law of the distribution for $i = 1$ near the right edge, see Fig. 11(b). This is the result of the approaching of ϵ to the right boundary of the area of our consideration marked in Figs. 1 and 2. We tested more distributions at $\epsilon = 0.24$ and observed that the deviation from the power law near $p_s = 1$ gets higher. But, nevertheless, we still can distinguish the CLVs localized on separated nodes by comparing the edge values of the distributions $\rho(0)$ and $\rho(1)$.

Thus the first CLVs, whose number we denote as V_s, are preferably localized on the nodes not synchronized with the Ph clusters. Notice that due to the symmetry there are more V_s localized vectors in the opposite end of the spectrum.

Since these CLVs have nonzero values mainly on a limited and permanent set of nodes whose number we denote as M_s, the number of these vectors have to be at least approximately equal to the number of these nodes, $V_s \approx M_s$. To verify it we generate different matrices **A** and find the separated nodes for it. Then we find CLVs and compute the relative frequency $P(p_s > 0.5)$, where p_s is computed as discussed above, see Eq. (21). The vector is treated as localized on the separated nodes when $P > 0.5$. The number of such vectors V_s as a function of the number of separated nodes M_s is plotted in Fig. 12. Since M_s and V_s are integers, the points of the plot will overlap each other. To avoid it and show the areas where the points fall more often as dense clouds we add random numbers $\xi \in (-0.2,0.2)$ to data: $M_s + \xi$ and $V_s + \xi$. Panel (a) shows nine data sets computed at $\epsilon = 0.13$, 0.17, and 0.22 for $N = 64$, 128, and 256. The points are fitted very well by the straight line $V_s = M_s$ that confirms the expected relation between the number of localized vectors and the number of separated nodes.

Figure 12(b) illustrates the scaling of M_s and V_s with the network size N. One sees that though different matrices **A** result in different M_s and V_s, the scaling

$$M_s^* = M_s/N, \quad V_s^* = V_s/N, \tag{22}$$

results in the gathering of points within the same ranges. It means that the number of nodes separated from the Ph clusters as well as the number of localized on them CLVs grow with N as $M_s \sim N$ and $V_s \sim N$. Notice that this agrees with previously discussed scaling of the number of nodes attached to the Ph clusters, see Eq. (7).

We also checked the signs of Lyapunov exponents corresponding to the localized CLVs. In all cases the localized CLVs had positive Lyapunov exponents and the total number of positive Lyapunov exponents was always higher then V_s.

B. Properties of localization nodes

The separated nodes where the first CLVs are localized have common specific feature related to the instantaneous square deviations of a node from its neighborhood,

$$\tau_n(t) = h_n^2(t). \tag{23}$$

where $h_n(t)$ is given by Eq. (2). Figure 9(c) shows the distributions of τ_n. One can see that the distributions at nodes 1, 2, and 6–9 have the maximum in zero and they decay monotonically. On contrary, the distributions at nodes with numbers $n \geqslant 10$ differ markedly: All of them are separated from zero, and in some cases they are multimodal.

Since nodes 3, 4, and 5 are the floating ones, as indicate corresponding values of η_n in Fig. 9(a), the forms of corresponding distributions of τ_n are ambiguous. On the one hand, the distribution at node 4 looks as that in nonfloating ones. However, the distributions in nodes 3 and 5 correspond to the situation when a node belong to a Ph cluster at $n \geqslant 10$.

This can be clarified by finding the clusters at short intervals, $\mathcal{T} = 20$. Performing the serial cluster detections with this $\mathcal{T}$ for the network in Figs. 5 and 9, we found that the separated nodes 1 and 2 as well as the nodes of the small FS clusters 6–9 can sometimes be attached to a Ph cluster, but approximately 90% of time they oscillate separately. Contrary to this, the floating node 3 is not synchronized with the Ph clusters only 0.0008% of time steps, and node 5 is separated 0.0002% of time steps. However, node 4 remains separated from Ph clusters during 0.0022% of time steps. Though this is still a very

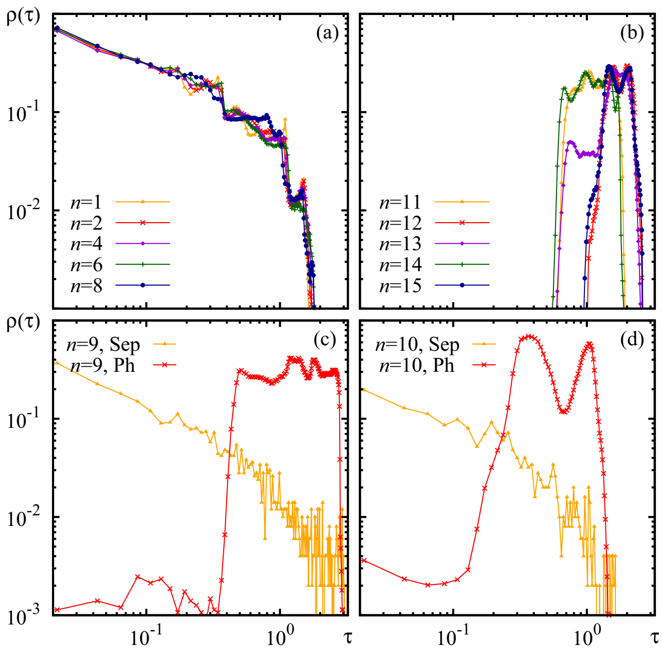

FIG. 13. (Color online) Distributions $\rho(\tau)$ at $N = 128, \epsilon = 0.13$ at different nodes n. The nodes are enumerated according to the growth of η_n, see Eq. (9). Panel (a) shows the separated nodes, while panel (b) corresponds to the nodes attached to the Ph clusters. Panels (c) and (d) demonstrate distributions at the floating nodes $n = 9$ and 10, respectively, computed independently when the node is separated (labeled "Sep" in the figure) and attached to the Ph clusters (label "Ph").

small value, it is one order higher than for nodes 3 and 5. Thus the form of the distribution of τ_n depends on the percentage of time that the node spends being not synchronized with the Ph clusters.

Figure 13 exemplifies the typical forms of the distributions of τ_n in more detail. A network generated to plot this figure had eight purely separated nodes and two floating ones. The nodes are assumed to be enumerated according to the growth of clustering index η_m, see Eq. (9). In Fig. 13(a) one can see that the distributions of τ_n at the separated nodes have a power-law shape near the origin and right after that it decays to zero, and, moreover, the shapes of the distributions in all of these nodes are almost identical. On the contrary, the distributions at the Ph cluster nodes are well separated from zero and can have multiple maxima, see Fig. 13(b). To plot the distribution for floating nodes in Figs. 13(c) and 13(d) we collected the data in two arrays; one was used when the node was attached to a Ph cluster, and the other when it was separated. One can see that, oscillating separately, the floating node demonstrates the power-law distribution of τ_n. The exponent coincides with the exponents of the distributions for purely separated nodes, cf. the slopes of the curves in Fig. 13(a) with the slopes of the corresponding curves in Figs. 13(c) and 13(d). When the floating node is attached to a Ph cluster its distribution corresponds in bulk to the distributions at purely cluster nodes, cf. the curves in Fig. 13(b) with the corresponding curves in Figs. 13(c) and 13(d). However, a remnant power-law tail near the origin can also be observed in Fig. 13(d).

One can see in Fig. 5 that each of the separated nodes where the first CLVs are localized has only one connection. This is typical for the localization nodes. Computing the connectivity degrees k_n in parallel with the data for Fig. 12, we found that, in most cases, $k_n = 1$, though rarely it can be higher. Nevertheless, the average connectivity degree of the separated nodes where CLVs are localized is less then 2.

Altogether, the first V_s CLVs are localized on M_s nodes. These nodes have specific properties: They are not synchronized with large Ph clusters, in most cases they have only one connection, and the distributions of τ_n at these nodes have identical power-law shapes. The core set of these nodes remains unchanged in course of the dynamics (however, there can exist a few so-called floating nodes). It means that this localization of CLVs is nonwandering. Since the localization nodes can be found without the straightforward computation of CLVs, we can predict where the first V_s CLVs are localized.

VI. SUMMARY AND CONCLUSION

In this paper we found that CLVs for a dynamical network can demonstrate nonwandering localization on nodes that can be found without the computation of CLVs. This is an example of explicit relations between dynamics of a system and the associated tangent-space dynamics.

Random scale-free dynamical networks of Hénon maps are considered. The networks are generated using a preferential attachment mechanism, and the resulting network always has N nodes and $N - 1$ connections.

The dynamics of such network is chaotic. Though the synchronization of the whole network is not observed, the nodes can form synchronized clusters. Full chaotic synchronization as well as phase synchronization are possible. The number of clusters depends on the coupling strength. We limit ourselves to a range of coupling strengths where there are two large phase clusters, including almost all nodes, and many small fully synchronized clusters. Most of the them are embedded into the phase clusters while few of them can be separated.

Due to the presence of clusters, covariant Lyapunov vectors are found to be localized. Each cluster of S_f fully synchronized nodes is associated with $2(S_f - 1)$ covariant vectors, all of whose sites are strictly zeros except for the nodes corresponding to the clusters. This localization is nonwandering and predictable since we can find nonzero vector sites without computing the covariant vectors. However, it is unclear which vector will be localized on the particular cluster.

One more mechanism of localization is related to the phase clusters. The first V_s CLVs are localized on M_s nodes that oscillate separately from the phase clusters. This localization is not quite as strict as the previous one, and the vectors can have nonzero sites on nodes attached to the phase clusters. But the probability of localization on separated nodes is always higher and this is the criterion for distinguishing these vectors. The number of vectors V_s and the number of separated nodes M_s are equal; however, since the localization is not strict, this equality is approximate. As well as the localization of clusters of full synchronization this is the nonwandering and predictable localization. Finding the nodes oscillating separately from the phase clusters we can say in advance where the first CLVs will be preferably localized and what will be their number. The nodes of localization have specific features: They have few connections (only one connection, in the cases), and they demonstrate identical power-law distributions of square deviations of dynamical variables from their neighborhood.

The *a priori* knowledge about the localization of the covariant vectors opens perspectives of wider utilization of these vectors. By the definition these vectors we show how the development of perturbations occurs. When the locations of areas of the most intensive development is permanent and predictable, an interesting problem arises regarding how to organize an effective low-energy forcing to the system using this areas.

Computing CLVs for the dynamical networks with full synchronization clusters, we found that both known methods can be not quite correct due the splitting of the tangent space into a set of time-invariant pairwise orthogonal subspaces. In view of the great interest of research into the dynamical networks a challenging task emerges regarding modification of the numerical methods for CLVs to fix this problem.

ACKNOWLEDGMENTS

P.K. thanks U. Parlitz for stimulating discussions. P.K. acknowledges the President RF program of support of leading Russian research schools (Grant No. NSh-1726.2014.2).

[1] K. Kaneko, Physica D **23**, 436 (1986).
[2] G. Giacomelli and A. Politi, Europhys. Lett. **15**, 387 (1991).
[3] M. Falcioni, U. M. Marconi, and A. Vulpiani, Phys. Rev. A **44**, 2263 (1991).
[4] G. P. Morriss, Phys. Rev. E **85**, 056219 (2012).
[5] F. Ginelli, P. Poggi, A. Turchi, H. Chaté, R. Livi, and A. Politi, Phys. Rev. Lett. **99**, 130601 (2007).
[6] C. L. Wolfe and R. M. Samelson, Tellus A **59**, 355 (2007).
[7] R. Buizza and T. N. Palmer, J. Atmos. Sci. **52**, 1434 (1995).
[8] Arkady S. Pikovsky and Jürgen Kurths, Phys. Rev. E **49**, 898 (1994); A. Pikovsky and A. Politi, Nonlinearity **11**, 1049 (1998).
[9] D. Pazó, I. G. Szendro, J. M. López, and M. A. Rodríguez, Phys. Rev. E **78**, 016209 (2008).
[10] I. G. Szendro, J. M. López, and M. A. Rodríguez, Phys. Rev. E **78**, 036202 (2008).
[11] A. Politi and A. Torcini, Chaos **2**, 293 (1992).
[12] A.-L. Barabási, R. Albert, and H. Jeong, Physica A **281**, 69 (2000).
[13] G. Benettin, L. Galgani, A. Giorgilli, and J. M. Strelcyn, Meccanica **15**, 9 (1980).
[14] I. Shimada and T. Nagashima, Prog. Theor. Phys. **61**, 1605 (1979).
[15] P. V. Kuptsov and U. Parlitz, J. Nonlinear Sci. **22**, 727 (2012).
[16] Sarika Jalan and R. E. Amritkar, Phys. Rev. Lett. **90**, 014101 (2003); S. Jalan, R. E. Amritkar, and Ch.-K. Hu, Phys. Rev. E **72**, 016211 (2005).
[17] A. Bergner, M. Frasca, G. Sciuto, A. Buscarino, E. J. Ngamga, L. Fortuna, and J. Kurths, Phys. Rev. E **85**, 026208 (2012).
[18] L. V. Gambuzza, A. Cardillo, A. Fiasconaro, L. Fortuna, J. Gomez-Gardenes, and M. Frasca, Chaos **23**, 043103 (2013).
[19] Ute Dressler, Phys. Rev. A **38**, 2103 (1988).
[20] A. J. Bosch, Am. Math. Month. **93**, 462 (1986).